TU Delft

Delft University of Technology

Document Version
Final published version

Citation (APA)
Schenken, W. K., Meynell, S. A., Machado, F., Ye, B., McLellan, C. A., Joos, M., Dobrovitski, V. V., Yao, N. Y., & Bleszynski Jayich, A. C. (2024). Long-lived coherences in strongly interacting spin ensembles. *Physical Review A*, *110*(3), Article 032612. https://doi.org/10.1103/PhysRevA.110.032612

Important note
To cite this publication, please use the final published version (if applicable).
Please check the document version above.

Copyright
In case the licence states “Dutch Copyright Act (Article 25fa)”, this publication was made available Green Open Access via the TU Delft Institutional Repository pursuant to Dutch Copyright Act (Article 25fa, the Taverne amendment). This provision does not affect copyright ownership.
Unless copyright is transferred by contract or statute, it remains with the copyright holder.

Sharing and reuse
Other than for strictly personal use, it is not permitted to download, forward or distribute the text or part of it, without the consent of the author(s) and/or copyright holder(s), unless the work is under an open content license such as Creative Commons.

Takedown policy
Please contact us and provide details if you believe this document breaches copyrights.
We will remove access to the work immediately and investigate your claim.

This work is downloaded from Delft University of Technology.

Green Open Access added to TU Delft Institutional Repository

'You share, we take care!' - Taverne project

https://www.openaccess.nl/en/you-share-we-take-care

Otherwise as indicated in the copyright section: the publisher is the copyright holder of this work and the author uses the Dutch legislation to make this work public.

Long-lived coherences in strongly interacting spin ensembles

William K. Schenken,[1,2,*] Simon A. Meynell,[2,*] Francisco Machado,[3,4] Bingtian Ye,[4] Claire A. McLellan,[2] Maxime Joos,[2] V. V. Dobrovitski,[5,6] Norman Y. Yao,[4] and Ania C. Bleszynski Jayich[2]

[1]*Department of Physics, University of Colorado, Boulder, Colorado 80309, USA*
[2]*Department of Physics, University of California, Santa Barbara, California 93106, USA*
[3]*ITAMP, Harvard-Smithsonian Center for Astrophysics, Cambridge, Massachusetts 02138, USA*
[4]*Department of Physics, Harvard University, Cambridge, Massachusetts 02138, USA*
[5]*QuTech, Delft University of Technology, Lorentzweg 1, 2628 CJ Delft, The Netherlands*
[6]*Kavli Institute of Nanoscience, Delft University of Technology, Lorentzweg 1, 2628 CJ Delft, The Netherlands*

(Received 28 September 2023; revised 12 January 2024; accepted 20 August 2024; published 12 September 2024)

Periodic driving has emerged as a powerful tool to control, engineer, and characterize many-body quantum systems. However, the required pulse sequences are often complex, long, or require the ability to control the individual degrees of freedom. In this work, we study how a simple Carr-Purcell–Meiboom-Gill (CPMG)-like pulse sequence can be leveraged to enhance the coherence of a large ensemble of spin qubits and serve as an important characterization tool. We implement the periodic drive on an ensemble of dense nitrogen-vacancy (NV) centers in diamond and examine the effect of pulse rotation offset as a control parameter on the dynamics. We use a single diamond sample prepared with several spots of varying NV density, which, in turn, varies the NV-NV dipolar interaction strength. Counterintuitively, we find that rotation offsets deviating from the ideal π pulse in the CPMG sequence (often classified as pulse errors) play a critical role in preserving coherence along an axis set by the π pulses even at nominally zero rotation offset. The cause of the coherence preservation is an emergent effective field that scales linearly with the magnitude of the rotation offset for small offsets. In addition to extending coherence, we compare the rotation offset dependence of coherence to numerical simulations to measure the disorder and dipolar contributions to the Hamiltonian to quantitatively extract the densities of the constituent spin species within the diamond.

DOI: 10.1103/PhysRevA.110.032612

I. INTRODUCTION

Engineered quantum systems have emerged as powerful and flexible tools for probing many-body physics. Whether composed of atomic, superconducting, or solid-state defect degrees of freedom, these platforms now routinely provide important insights into myriad phenomena such as phases of matter [1–5] and quantum decoherence [6–10], and can even enable the generation of metrologically useful entangled states [11–16]. The physics of these many-body phenomena crucially depends on the interplay between two distinct types of interactions: those within the system itself (internal) and those between the system and its environment (external). Hence, controlling and characterizing these interactions is central to developing a many-body quantum simulator or a sensor.

Defects in semiconductors such as diamond—in particular, the nitrogen-vacancy (NV) center—are especially promising as a platform for exploring many-body physics owing to their optical polarizability and their ability to access large system sizes [4,6,21,22]. While it has recently become possible to synthesize ensembles of dipolar interacting NV centers [6,23,24], additional interactions with the environment often destroy the system's coherence, limiting the landscape of explorable quantum many-body phenomena. For example, other defects in the diamond lattice, such as the spin-1/2 substitutional nitrogen impurity (P1 centers) or NV centers of other orientations, introduce a local, random, fluctuating magnetic field; such fluctuations are typically the primary source of decoherence in NV systems. To design and realize novel many-body states in NV ensembles and gain a clear understanding of decoherence pathways, it is important to characterize the various interactions within the system and between the system and its environment. Armed with this information, suitable protocols can be used to either mitigate [25,26] or leverage [27] these interactions.

One powerful method to probe and manipulate interactions in spin systems is Hamiltonian engineering, where the spins are manipulated via coherent pulses on a timescale faster than any interaction strength present in the system, resulting in an effective time-averaged Hamiltonian $\bar{H}$ that describes the evolution of the spins. Through fine tuning of the pulse sequence parameters (i.e., rotation angle, rotation axes, pulse duration, timing between pulses), the effective Hamiltonian can be engineered to extend coherence by decoupling external disorder (e.g., Hahn echo [28] or CPMG [29,30]) or suppressing internal interactions (e.g., WAHUHA [31]). Recently, complex sequences have been designed that are capable of suppressing both disorder and interactions while being robust to

[*]These authors contributed equally to this work.

 ©2024 American Physical Society

pulse errors (DROID [32]). Outside of dynamical decoupling, Hamiltonian engineering has also been applied to simulating many-body physics in engineered spin systems [27].

In this paper, we demonstrate how replacing π pulses with $\pi + \epsilon$ pulses in the canonical CPMG sequence, which we dub the ϵ-CPMG sequence, provides a simple yet powerful scheme for controlling the system's effective Hamiltonian. This control manifests itself in the ability to engineer the relative strength between onsite disorder and dipolar interactions in a pulse-error-robust fashion. Using this simple ϵ-CPMG sequence, our observations are twofold. First, moving away from the CPMG sequence, i.e., $\epsilon \neq 0$, leads to a surprising extension of spin coherence out to timescales approaching the spin-locking timescale, $T_{1,\rho}$, regardless of the ratio of dipolar interactions to disorder. Second, the robust control over the effective Hamiltonian offers a novel yet simple way of experimentally characterizing the strength of dipolar interactions and disorder, an important characteristic of many-body systems. Crucially, this understanding can be transferred into a quantitative measure of the density of spin defects, both the NV and surrounding spin baths.

II. EFFECT OF ROTATION OFFSETS

We investigate a chemical vapor deposition (CVD)-grown diamond sample (sample C041) with a several-μm thick nitrogen-doped layer, as detailed in previous work [23]. As schematically indicated in Fig. 1(a), the diamond was irradiated in several-μm-scale spots with electrons of varying dosage and energy. A key feature of our sample is that in the spots with higher irradiation dosage, the NV density is high enough to play a significant role in the decoherence dynamics [23]. The NV dynamics are governed by the following Hamiltonian,

$$H = \sum_i B_i^z(t)\sigma_i^z + \sum_{i<j} J_{ij}\left(\sigma_i^x\sigma_j^x + \sigma_i^y\sigma_j^y - \sigma_i^z\sigma_j^z\right), \qquad (1)$$

where the first summand is referred to as disorder or external interactions, the second summand contains the dipolar or internal interactions, $B_i^z(t)$ is the local on-site field at spin i, which can vary as a function of time, t. The dipolar coupling between spins i and j is J_{ij}, and $\sigma_i^{x,y,z}$ are the Pauli spin operators for the ith spin. Our engineered Hamiltonian approach permits the characterization of these internal and external interactions without necessitating arbitrary wave generators (for fast and precise control) or multiple microwave drives (as in double resonance techniques). Instead, our ϵ-CPMG sequence [shown in the inset for Fig. 1(b)] varies a single parameter ϵ, defined as the deviation from a perfect π pulse. Additional experimental details can be found in the Appendices. An example of a long-lived coherence (transverse magnetization $\langle\sigma^y(t)\rangle$ [33]) resulting from this sequence is shown in Fig. 1(b).

Even though in Fig. 1(b), data is taken at a target of $\epsilon = 0$, a finite ϵ is still present due to experimental imperfections and is, indeed, the origin of the long-lived coherence. To elucidate the connection between finite ϵ and the long-lived coherence, we compare the results from the CPMG sequence to two different sequences designed to cancel the effects of accumulating pulse errors: an alternating-phase CPMG

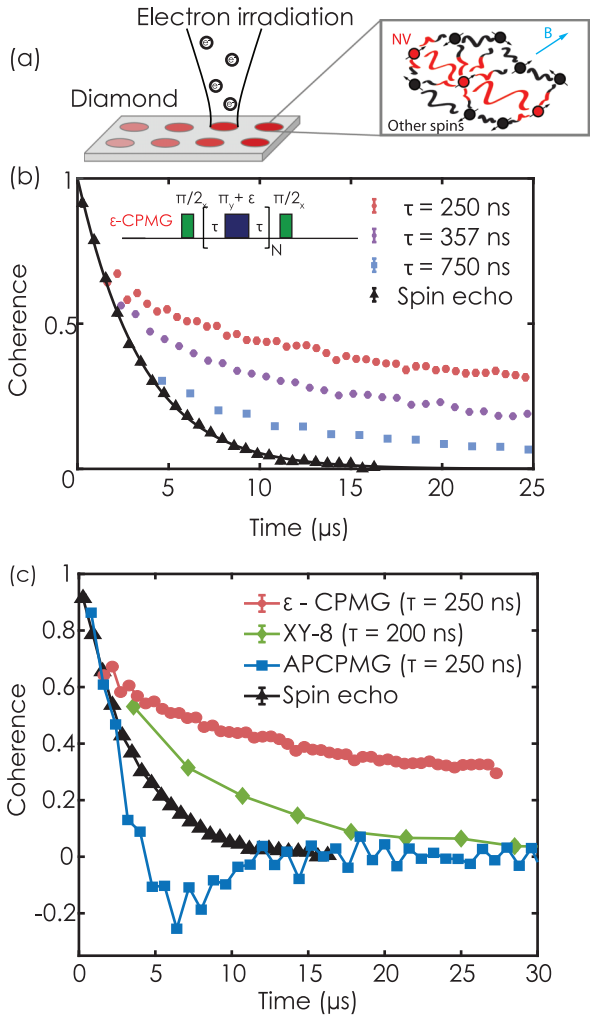


FIG. 1. Measurement of long-lived coherences in a dense NV ensemble. (a) Cartoon sketch of our spin system, a CVD-grown, nitrogen-doped diamond sample showing spots that have undergone localized electron irradiation of varying dosage, resulting in high NV densities that vary across spots. The NV ensemble (red) is mixed randomly with a bath of spins (black). A magnetic field (blue) is applied along the 111 direction. (b) Long-lived coherences observed under ϵ-CPMG. For the data shown, $\theta \approx \pi$, and N is varied for various fixed values of τ. For comparison, the spin echo is also shown ($N = 1$, $\theta \approx \pi$, variable τ). Data is taken on spot A [see Table I and Fig. 2(a)]. Details of the fit to the spin echo data are given in the Appendices. (c) Comparison of ϵ-CPMG to APCPMG (which has the same filter function [17–19]) and XY-8, elucidating the importance of a finite ϵ for preserving coherence in the ϵ-CPMG sequence ($\tau = 250$ ns). Both APCPMG and XY-8 [20] are designed to cancel the effect of accumulating rotation offsets. The experimental data shows a marked difference in coherence between ϵ-CPMG and the two sequences, reinforcing the notion that the finite, uncontrolled ϵ in the CPMG sequence is the origin of the state's long-lived nature. The APCPMG coherence decays faster than the XY-8 coherence, likely due to its susceptibility to frequency offsets such as those due to on-site disorder. Even though $\epsilon = 0$ is targeted in all cases, a finite rotation offset still exists. For reference, a spin echo sequence is shown in black.

(APCPMG) sequence and an XY-8 sequence. The CPMG sequence (red) shows substantially longer coherence times

TABLE I. Comparison of spin densities for spots A, B, and L as obtained from instantaneous diffusion (ID), DEER (Ref. [23]) and from ϵ-CPMG, showing good agreement in the NV density. Explanations for the discrepancies are discussed in the text.

Spot	Dosage	Energy	$[NV]_{ID}$	$[P1]_{DEER}$	$[NV]_{\epsilon-CPMG}$	$[spin\text{-}defect]_{\epsilon\text{-}CPMG}$
A	10^{21} (e^-/cm^2)	200 keV	2.7 ± 0.08 ppm	3.8 ± 0.2 ppm	2.1 ± 0.3 ppm	23.2 ± 0.5 ppm
B	10^{20} (e^-/cm^2)	200 keV	2.2 ± 0.21 ppm	10.5 ± 0.2 ppm	1.3 ± 0.4 ppm	17.4 ± 0.9 ppm
L	10^{22} (e^-/cm^2)	145 keV	1.0 ± 0.2 ppm	–	0.6 ± 0.3 ppm	16.1 ± 0.7 ppm

than both the XY-8 and the APCPMG sequence. Indeed, we expect that the XY-8 data provides a more accurate assessment of the dipolar-induced coherence decay and thus emphasizes the importance of pulse errors in extending the coherence of ϵ-CPMG, even beyond the dipolar limit. In nuclear spin systems [34,35], finite pulse duration has been used to explain a similar difference between CPMG and APCPMG.[1] Strongly interacting spin systems in silicon [36] have demonstrated a similar enhancement of coherence at finite ϵ during CPMG, with their optimal value being ten degrees.

III. EFFECTS OF DIPOLAR INTERACTIONS AND DISORDER

Next, we examine three distinct irradiated spots on sample C041, whose details are shown in Table I. We also study the unirradiated background, where the NV density is sufficiently low, such that NV-NV interactions are negligible. In Fig. 2, we plot the coherence of multiple different NV ensembles subject to our ϵ-CPMG pulse sequence as a function of ϵ for $\tau = 250$ ns. The results demonstrate how this one simple knob can be tuned to optimize coherence for different spin environments, realized in the differently irradiated spots [Fig. 2(a) and Table I]. Figure 2(b) shows that in the lowest NV density spot (spot BG) coherence is maximized for $\epsilon = 0$, as in an ideal CPMG sequence. At $\epsilon = 90$ degrees the coherence drops to about half its maximum value. As the NV density increases in spots L, B, and A, internal dipolar interactions start to dominate the decoherence dynamics at small ϵ, leading to a double-humped feature where coherence is maximized at a nonzero ϵ.

The effective Hamiltonian under the train of pulses has particularly simple intuition for two extremal values of ϵ: when $\epsilon = 0$, i.e., a conventional CPMG sequence, static disorder is decoupled [28–30,37] and dipolar couplings are unaffected (the dipolar interaction between two spins is invariant under a π rotation of both spins); when $\epsilon = \pm\pi/2$, the dipolar interactions between NVs are maximally averaged out [38] while the static disorder is only averaged out half as effectively as in the $\epsilon = 0$ case. When both static disorder and dipolar interactions are present, an intermediate ϵ is best suited to maximizing the coherence in such cases. Measuring NV ensemble coherence as a function of ϵ and N determines the strength of dipolar coupling relative to disorder.

Having understood the features of the sequence at large N, we next examine the system's coherence as a function of the number of pulses, N. Figure 2(c) shows coherence vs. ϵ in spot A for a varying number of pulses, N, while keeping the interpulse spacing constant. Qualitatively, we observe the emergence and deepening of a coherence dip at $\epsilon = 0$ as N increases. Coherence is also lost at higher N due to the increased duration of the pulse sequence. After ~5 pulses, the dip is clearly visible. Using a simple analytical model to compute the system's late-time coherence, we reproduce the experimental observations and find good agreement with the relative strength between interactions and disorder. We find that the periodic drive gives rise to an ϵ-dependent effective magnetic field along the y direction that suppresses depolarization. This effective magnetic field is linear for angles that are small compared to 1 radian. Crucially, for this sequence, the spins are initialized in the y direction. In dense ensembles of nuclear spins, Refs. [39,40] have observed behavior similar to Fig. 2.

While an approximate effective Hamiltonian description of the data, as detailed in the Appendices, provides physical intuition, it fails to provide a direct and quantitative mapping between the properties of the sample and the observed dynamics. We tackle this gap by simulating the full dynamics of the NV ensemble interacting with a bath of spin-1/2 defects. Crucially, this approach enables us to capture the full extent of the experimental observations (both as a function of angle error ϵ and number of pulses N) and use the agreement between

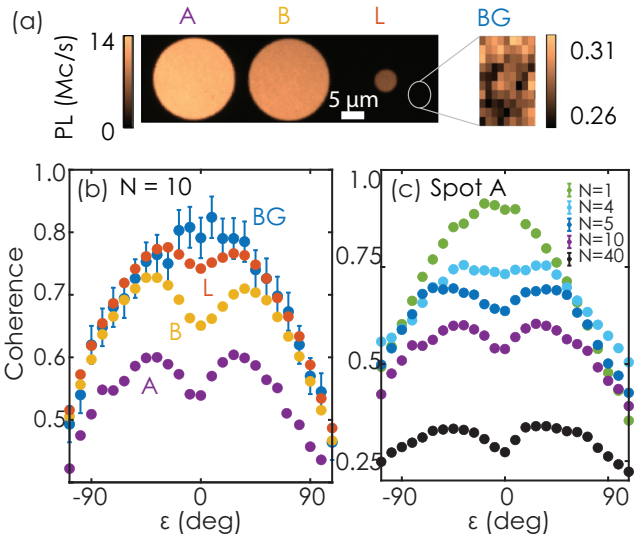


FIG. 2. Behavior of ϵ-CPMG sequence. (a) Confocal images of spots A, B, and L, showing a range of brightness indicating a range of NV densities. (b) Coherence versus ϵ for various NV densities at fixed $N = 10$ and $\tau = 250$ ns, and (c) for various N for a given NV density (spot A) and τ. See the Appendices for a comparison of this data to an analytic model.

[1]In our numerical analysis, we include the effects of dipolar interactions during the pulse, finite pulse duration, and rotation offset.

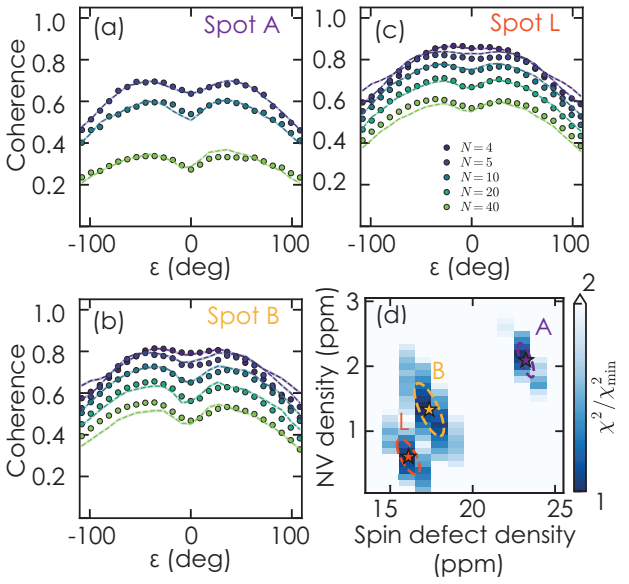


FIG. 3. Simulations of long-lived coherences. (a), (b), (c) Coherence versus ϵ for various N and for spots A, B, L. Markers show experimental data. Plotted as dashed lines are the numerics for the parameters $\{\rho_{NV}, \rho_{\text{bath}}\}$ that minimized χ^2. (d) χ^2 contour plots as a function of ρ_{NV} and ρ_{bath}. The color maps for each spot have been superimposed. Separated colormaps are shown in the Appendices.

numerical data and experiments to quantitatively characterize important features of the sample such as the density of different spin defects, thus revealing the relative strengths of disorder and interactions.

To this end, we compute the dynamics of an NV ensemble with density n_{NV} surrounded by a bath of defects at density n_{bath}. See the Appendices for an explanation of the numerical methods. By computing the NV ensemble dynamics over different sets of densities of NVs and bath spins $\{n_{\text{NV}}, n_{\text{bath}}\}$ and averaging over different spatial configurations of the NV and bath ensembles [41,42], we obtain the coherence dynamics for a wide range of samples as a function of ϵ and N. We compare the resulting coherence dynamics across different $N : N > 3$ for each pair of parameters,[2] $\{n_{\text{NV}}, n_{\text{bath}}\}$, estimating the agreement between numerical and experimental data via a χ^2-like measure.

IV. DISCUSSION

Sample fits and χ^2 contour plots are shown in Fig. 3. We find that there is a clear region within this parameter space that minimizes χ^2. The corresponding densities are shown in Table I. The extracted NV densities match the trends of those measured on the same sample via DEER and instantaneous diffusion [23], with the precise values falling within or just outside their respective error bars. The spin bath density reported here is larger than the P1 density obtained via DEER, primarily because the present method is sensitive to all spinful defects in the diamond, not just to P1s, whereas DEER is, by design, only sensitive to a single group of P1 centers.[3] Our simulations also give an NV density slightly lower than what was reported previously from instantaneous diffusion measurements [23]. The previous analyses necessitated several approximations, such as a quasistatic spin bath in the case of DEER and a dominant NV bath in the case of instantaneous diffusion. The present numerical treatment is free from these assumptions and, hence, is a more reliable probe of the NV density.

We stress that our ability to quantitatively extract the densities of competing disordered and dipolar spin baths harbors key advantages over other methods such as DEER, XY-8, and instantaneous diffusion, namely technical simplicity, robustness to pulse errors in the form of rotation offsets, and the ability to simultaneously probe both NV density and disorder without assuming one to be dominant.

Using DEER to measure total disorder requires addressing each individual bath spectrally and is hampered by factors such as inhomogeneous broadening and fast-varying noise. Measuring dipolar couplings via NV-NV DEER is also possible, but only for high-density ensembles and significant engineering to control the alignment of RF fields with the different NV groups. Instantaneous diffusion can be used to measure the strength of the dipole-dipole interaction via the extension of T_2 under non-π pulses but cannot easily measure disorder and assumes that the change in T_2 with pulse angle is unrelated to the change in coupling to disorder. Using decoupling techniques such as XY-8 or DROID [24] and comparing the coherence times between dipole-decoupled and disorder-decoupled is another way to assess the relative importance between these terms. Though XY-8 and DROID are better at preserving arbitrary initial states (the ϵ-CPMG sequence is best at preserving a state prepared along the direction of the effective field), XY-8 and DROID require complex sequencing, and quantifying the strength of disorder versus dipolar interactions is challenging. In this paper, we have shown how the ϵ-CPMG sequence extends the coherence of spin ensembles to times approaching $T_{1,\rho}$ and provides quantitative information about the relative strengths of dipolar interactions and disorder, important figures of merit for many-body systems. Further, we show how our approach to Hamiltonian engineering can tune from dipolar-dominated to disorder-dominated physics. Using this tunability, we identify an optimal ϵ for maximizing coherence of an NV ensemble. We benchmark our pulse sequence, its ability to tune interaction strengths, and our numerical methods for estimating spin densities on a single sample with multiple different NV densities.

V. CONCLUSION

As decoherence mitigation becomes an increasingly large scientific endeavor, fast, straightforward, and accurate diagnostic sequences like the one presented here will become ever more essential for understanding how many-body quantum systems decohere. Fast and efficient characterization of

[2]The observations for the first few cycles, $N \leqslant 3$, are expected to depend on the details of the initialization process, which we do not capture in our simulation.

[3]These extra spinful defects could be a result of the high irradiation dosage.

quantum systems may become increasingly important in the pipeline for creating and developing samples; we propose that the ϵ-CPMG sequence represents one such way of mitigating this potential bottleneck because it is efficient, has a small technical footprint, and is unambiguous in its diagnosis. Moreover, while we expect that ϵ-CPMG will be primarily applicable to solid-state systems, we note that the treatment is generic and could be applied to systems beyond dense NV ensembles; in any disordered system where the nature of interactions between particles within the system and without must be understood, we expect ϵ-CPMG to be useful. Finally, we anticipate that this framework may be extended beyond a two-component Hamiltonian by introducing additional tuning parameters within a periodic drive (for example, ϵ_x for x pulses and ϵ_y for y pulses) to extend this treatment to even more complicated Hamiltonians.

ACKNOWLEDGMENTS

We gratefully acknowledge support of the Army Research Office through the MURI program Grant No. W911NF-20-1-0136, the U.S. Department of Energy BES Grant No. DE-SC0019241, and the DARPA DRINQS program (contract D18AC00015KK1934 and D18AC00033). This work is part of the research programme NWO QuTech Physics Funding (QTECH, programme 172) with Project No. 16QTECH02, which is (partly) financed by the Dutch Research Council (NWO). W.K.S. acknowledges support from the NDSEG Fellowship. S.A.M. acknowledges support from the UCSB Quantum Foundry (NSF DMR-1906325) and support from the Canada NSERC (Grant No. AID 516704-2018). F.M. acknowledges support from the NSF Award No. 2116679 through a grant for ITAMP at Harvard University.

APPENDIX A: SAMPLE PREPARATION AND MEASUREMENT

To tune electron density we use a commercial TEM as in Ref. [23]. The TEM electron irradiation creates vacancies, and an 850 °C anneal promotes the conversion of nitrogen to NV centers. By tuning the dosage, we can tune the relative strength of NV-NV interactions from spot to spot.

After optical polarization into $|0\rangle$ using a 532 nm green laser, a microwave $\pi/2$ pulse in the x direction initializes the spins into the state $|+y\rangle$. Then, with a CPMG-like train of pulses, the spins undergo repeated rotations about the $+\hat{y}$ axis by an angle $\theta = \pi + \epsilon$. At the end of the sequence, the NVs are mapped into a population by a final $\pi/2$ pulse along the x direction, and the state is read out optically via spin-dependent photoluminescence under a 532 nm laser pulse. All measurements presented are performed in a ∼320 G magnetic field aligned with one of the four NV axes. Microwave (MW) pulses address the $\{|0\rangle, |-1\rangle\}$ transition of the aligned NV group.

The data in Fig. 1(b) was fit to an exponential, $\exp(t/T_2)^n$ with $n = 1$ and $T_2 = 3.5\,\mu$s. This is consistent with the expected exponent in Ref. [6] for high conversion efficiencies where the physics is expected to follow an NV-NV Ramsey-type exponential. We used rectangular pulses with a Rabi frequency of $\Omega = 2\pi \times 11.9$ MHZ throughout the experiments in this paper. The $T_2{}^*$ in Spot A as measured via Ramsey decay is 340 ns.

APPENDIX B: EPSILON DEPENDENCE OF THE COHERENCE

To gain some intuition for the qualitative shape of the coherence vs. ϵ, we present a theoretical analysis of the coherence after ten pulses. We analyze each of the three spots using this treatment and show that the strength of the dip corresponds to a term proportional to the variance of the dipole-dipole coupling, $\langle J_{i,j}^2 \rangle$.

To derive an effective, time-independent Hamiltonian, we examine the time-evolution operator over two cycles, given a native Hamiltonian, $H = \sum_i B_i^z \sigma_i^z + \sum_{i<j} J_{ij}(\sigma_i^x \sigma_j^x + \sigma_i^y \sigma_j^y - \sigma_i^z \sigma_j^z) = H_{\text{on-site}} + H_{\text{dipolar}}$.

$$\hat{U}^2 = e^{-iH\tau} R_y(\pi+\epsilon) e^{-2iH\tau} R_y(\pi+\epsilon) e^{-iH\tau} \tag{B1}$$

$$= e^{-iH\tau} R_y(\epsilon) e^{-2i\tilde{H}\tau} R_y(\epsilon) e^{-iH\tau}, \tag{B2}$$

where $R_y(\theta)$ is the rotation operator about the y direction by an angle, θ and $\tilde{H} = R_y(\pi) H R_y(\pi) = -H_{\text{on-site}} + H_{\text{dipolar}}$. $B_i{}^z$ is the z field for spin i and assumed to be time independent for this analysis. For the numerical treatment in the main text, we relax this assumption and allow a time-varying field. We then find an effective time-independent Hamiltonian using the Magnus expansion focusing on the region close to $\epsilon = 0$ because this is the regime where the effects of finite $J_{i,j}$ are most pronounced.

Our zeroth-order term will be given by,

$$H_{\text{eff}}^{(0)} = \frac{2\epsilon \sum \sigma_i^y}{4\tau} + H_{\text{dipole}} = B_{\text{eff}} \sum_i^M \sigma_i^y + H_{\text{dipole}}, \tag{B3}$$

where $B_{\text{eff}} = \epsilon/2\tau$. Higher-order terms will be generated by the commutators between H, $\frac{\epsilon\sigma^y}{\tau}$, and $\tilde{H}$.

We measure the average coherence along the y direction, averaged over the M addressed NV centers. After equilibrating, the coherence, C, will be given by,

$$C = \frac{1}{M}\left\langle \sum_i^M \sigma_i^y \right\rangle = \frac{1}{M} \text{tr}\left[\sum_i^M \sigma_i^y e^{-\beta H_{\text{eff}}} \right] \Big/ Z$$

$$\approx \frac{-\beta}{MZ} \text{tr}\left[\sum_i^M \sigma_i^y H_{\text{eff}}^{(0)} \right] = \frac{-\beta B_{\text{eff}}}{Z}. \tag{B4}$$

We use, $\rho = e^{-\beta H_{\text{eff}}}/Z$, where Z is the partition function and β is given by an effective spin temperature, $\beta = 1/k_B T$ that satisfies $\beta H_{\text{eff}} \ll 1$.

The temperature is determined by the initial value of the y magnetization, which is initialized such that $C = 1$, as detailed in the main text. We relate the initial and final energies through

$$\sum_i^M B_{\text{eff}} = \langle H_{\text{eff}} \rangle \approx \frac{-\beta}{Z} \text{tr}\left[H_{\text{eff}}^2\right]. \tag{B5}$$

Using Eqs. (B4) and (B5), we arrive at the expression,

$$C = \frac{M B_{\text{eff}}^2}{\text{tr}\left[H_{\text{eff}}^2\right]}. \tag{B6}$$

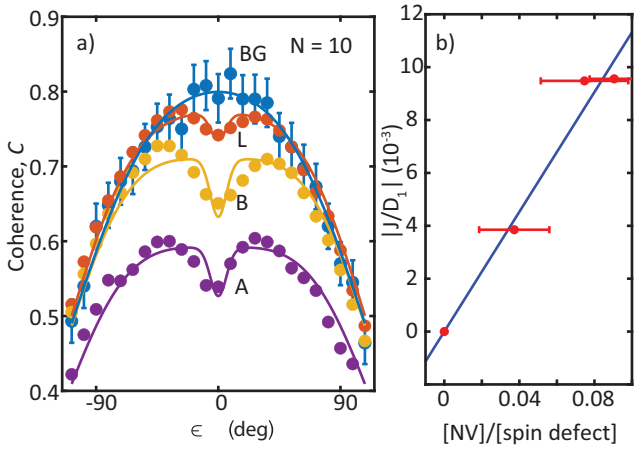


FIG. 4. (a) Comparison of the coherence as a function of ϵ across different spots to an analytical model that parameterizes the curves in terms of J. (b) A comparison of the fit parameter J/D_1 to the ratio of the NV density to the spin defect density obtained via numerical modeling in the main text. These have the expected linear relationship.

Finally, to arrive at an expression for $\mathrm{tr}[H_{\mathrm{eff}}^2]$, we examine lowest-order terms and expand about $\epsilon = 0$. This results in the following expression,

$$\begin{aligned}\mathrm{tr}[H^2] &= \mathrm{tr}\left[H_{\mathrm{dipolar}}^2\right] + \mathrm{tr}\left[\sum_i^M \left(B_{\mathrm{eff}}\sigma_i^y\right)^2\right] + \text{higher-order terms} \\ &= M\left(J^2 + B_{\mathrm{eff}}^2\right) + \text{higher-order terms} \\ &= M\left(J^2 + D_1^2\epsilon^2 + D_2^2\epsilon^4 + D_3^2\epsilon^6\right), \end{aligned} \tag{B7}$$

where $D_{1,2,3}$ are fit coefficients. Using Eqs. (B6) and (B7) and simplifying in terms of unique fit parameters, we have:

$$C = \frac{A\epsilon^2}{(J/D_1)^2 + \epsilon^2 + (D_2/D_1)^2\epsilon^4 + (D_3/D_1)^2\epsilon^6}. \tag{B8}$$

The typical value of the dipolar coupling J, as defined in Eq. (B7), should be understood as a local value, characterizing only a region of the sample with finite lattice spacing. Indeed, the quantity $\mathrm{tr}H_{\mathrm{dipolar}}^2$ diverges if averaging is performed over a macroscopic three-dimensional ensemble of rare spins where the spin-spin spacing is allowed to go to zero [41–44]. However, this quantity becomes finite and well determined if defined for a region of the sample where the spin-spin spacing is lower bounded. We note that the expression for B_{eff} shown here is valid for small ϵ (compared to 1 radian), as ϵ becomes large, the effective field will no longer be a monotonic function of ϵ.

The fits using this model across varying spot densities are shown in Fig. 4(a). We use a Gaussian smoothing of six degrees to account for the random uncertainties in pulse rotation caused by pulse-to-pulse variation and inhomogeneities over the confocal spot. The parameter (J/D_1) relates the strength of the dipolar contribution to other terms, including B_{eff} and qualitatively controls the strength of the dip about $\epsilon = 0$. We compare J/D_1 to the numerically extracted ratio of NV density to spin defect density and find that the two have the expected linear relationship.

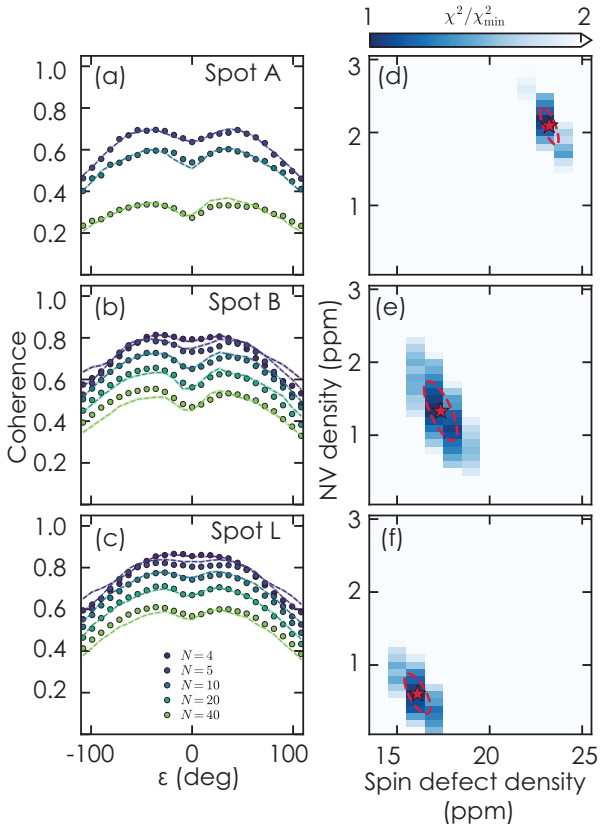


FIG. 5. Simulations of long-lived coherences as in the main text with the color maps, (d), (e), (f) separated instead of superimposed.

In this analysis, we consider offsets arising from incomplete angular rotations about the y axis. Frequency detuning can also result in rotation offsets and rotation about slightly different axes. We assume this effect is small for our experiments because the Rabi frequency is much larger than the linewidth. Crucially, unlike the APCPMG sequence, deviations from this effect do not accumulate with increasing pulse number as for rotation offsets in ϵ-CPMG.

APPENDIX C: NUMERICAL METHODS

The NVs are all initialized in the $|+y\rangle$ orientation, and their subsequent dynamics have three contributions: (i) dipolar interactions between NVs, (ii) Larmor precession arising from local, random magnetic fields generated by the bath spins, and (iii) periodic rotations by $\pi + \epsilon$ about the $\hat{y}$ axis. By contrast, the bath spin defects are assumed to be randomly polarized in either $\pm 1/2$ and exhibit no coherent dynamics. Instead, we consider their dynamics as a stochastic process that flips the polarization of the spin defect with some characteristic timescale, giving each spin in the bath a correlation time τ_c that is related to the density of the spin bath, as described in Ref. [8]. Such bath dynamics are crucial to capture the observed decoherence dynamics of the NV centers; without them, the effect of the spin bath can be exactly canceled for

perfect π pulses. In addition, we incorporate different experimental effects into the numerics, such as finite pulse duration, which are difficult to incorporate in a simple theoretical analysis.[4] The fits using this approach are shown in Fig. 5 with the color maps separated rather than superimposed as in the main text.

[4]Average Hamiltonian theory has been used to show that a finite pulse duration gives rise to effects similar to those studied here. For a detailed analysis of the effect of finite pulses, see Ref. [34].

We determine the best fit via minimization of a χ^2-like metric calculated as

$$\chi^2(\rho_{\mathrm{NV}}, \rho_{\mathrm{P1}}) = \sum_{N,\epsilon} [C_{\mathrm{data}}(\epsilon, N) - C_{\mathrm{fit}}(\epsilon, N, \rho_{\mathrm{NV}}, \rho_{\mathrm{P1}})]^2, \tag{C1}$$

where $C(\epsilon, N)$ denotes the coherence as a function of ϵ and the number of pulses, N. The plots shown in the text are normalized to the minimum of $\chi^2(\rho_{\mathrm{NV}}, \rho_{\mathrm{P1}})$. The densities of defects, $\rho_{\mathrm{NV}}, \rho_{\mathrm{P1}}$ are treated as fit parameters in the numerics. We use a doubling of χ^2 as our bounds for a region of reasonable fit. We note that the optimal ϵ is not uniquely determinative for the ratio of dipolar interaction strength. Instead, fitting the coherence as a function of both ϵ and N is required because the optimal ϵ can change as a function of N; thus multiple curves for multiple values of N are required.

[1] D. A. Abanin, E. Altman, I. Bloch, and M. Serbyn, Colloquium: Many-body localization, thermalization, and entanglement, Rev. Mod. Phys. **91**, 021001 (2019).

[2] J. Smith, A. Lee, P. Richerme, B. Neyenhuis, P. W. Hess, P. Hauke, M. Heyl, D. A. Huse, and C. Monroe, Many-body localization in a quantum simulator with programmable random disorder, Nat. Phys. **12**, 907 (2016).

[3] N. Y. Yao, M. P. Zaletel, D. M. Stamper-Kurn, and A. Vishwanath, A quantum dipolar spin liquid, Nat. Phys. **14**, 405 (2018).

[4] S. Choi, J. Choi, R. Landig, G. Kucsko, H. Zhou, J. Isoya, F. Jelezko, S. Onoda, H. Sumiya, V. Khemani, C. von Keyserlingk, N. Y. Yao, E. Demler, and M. D. Lukin, Observation of discrete time-crystalline order in a disordered dipolar many-body system, Nature (London) **543**, 221 (2017).

[5] G. Kucsko, S. Choi, J. Choi, P. C. Maurer, H. Zhou, R. Landig, H. Sumiya, S. Onoda, J. Isoya, F. Jelezko, E. Demler, N. Y. Yao, and M. D. Lukin, Critical thermalization of a disordered dipolar spin system in diamond, Phys. Rev. Lett. **121**, 023601 (2018).

[6] E. J. Davis, B. Ye, F. Machado, S. A. Meynell, W. Wu, T. Mittiga, W. Schenken, M. Joos, B. Kobrin, Y. Lyu, Z. Wang, D. Bluvstein, S. Choi, C. Zu, A. C. B. Jayich, and N. Y. Yao, Probing many-body dynamics in a two-dimensional dipolar spin ensemble, Nat. Phys. **19**, 836 (2023).

[7] B. L. Dwyer, L. V. H. Rodgers, E. K. Urbach, D. Bluvstein, S. Sangtawesin, H. Zhou, Y. Nassab, M. Fitzpatrick, Z. Yuan, K. De Greve, E. L. Peterson, H. Knowles, T. Sumarac, J.-P. Chou, A. Gali, V. Dobrovitski, M. D. Lukin, and N. P. de Leon, Probing spin dynamics on diamond surfaces using a single quantum sensor, PRX Quantum **3**, 040328 (2022).

[8] E. Bauch, S. Singh, J. Lee, C. A. Hart, J. M. Schloss, M. J. Turner, J. F. Barry, L. M. Pham, N. Bar-Gill, S. F. Yelin, and R. L. Walsworth, Decoherence of ensembles of nitrogen-vacancy centers in diamond, Phys. Rev. B **102**, 134210 (2020).

[9] A. Buchleitner and A. R. Kolovsky, Interaction-induced decoherence of atomic bloch oscillations, Phys. Rev. Lett. **91**, 253002 (2003).

[10] S. Takahashi, I. S. Tupitsyn, J. van Tol, C. C. Beedle, D. N. Hendrickson, and P. C. E. Stamp, Decoherence in crystals of quantum molecular magnets, Nature (London) **476**, 76 (2011).

[11] T.-X. Zheng, A. Li, J. Rosen, S. Zhou, M. Koppenhöfer, Z. Ma, F. T. Chong, A. A. Clerk, L. Jiang, and P. C. Maurer, Preparation of metrological states in dipolar-interacting spin systems, npj Quantum Inf. **8**, 150 (2022).

[12] Y. Chu, X. Li, and J. Cai, Strong quantum metrological limit from many-body physics, Phys. Rev. Lett. **130**, 170801 (2023).

[13] J. A. Hines, S. V. Rajagopal, G. L. Moreau, M. D. Wahrman, N. A. Lewis, O. Marković, and M. Schleier-Smith, Spin squeezing by Rydberg dressing in an array of atomic ensembles, Phys. Rev. Lett. **131**, 063401 (2023).

[14] G. Bornet, G. Emperauger, C. Chen, B. Ye, M. Block, M. Bintz, J. A. Boyd, D. Barredo, T. Comparin, F. Mezzacapo, T. Roscilde, T. Lahaye, N. Y. Yao, and A. Browaeys, Scalable spin squeezing in a dipolar Rydberg atom array, Nature **621**, 728 (2023).

[15] W. J. Eckner, N. D. Oppong, A. Cao, A. W. Young, W. R. Milner, J. M. Robinson, J. Ye, and A. M. Kaufman, Realizing spin squeezing with Rydberg interactions in a programmable optical clock, Nature **621**, 734 (2023).

[16] J. Franke, S. R. Muleady, R. Kaubruegger, F. Kranzl, R. Blatt, A. M. Rey, M. K. Joshi, and C. F. Roos, Nature **621**, 740 (2023).

[17] M. J. Biercuk, A. C. Doherty, and H. Uys, Dynamical decoupling sequence construction as a filter-design problem, J. Phys. B: At., Mol. Opt. Phys. **44**, 154002 (2011).

[18] C. L. Degen, F. Reinhard, and P. Cappellaro, Quantum sensing, Rev. Mod. Phys. **89**, 035002 (2017).

[19] L. Cywiński, R. M. Lutchyn, C. P. Nave, and S. Das Sarma, How to enhance dephasing time in superconducting qubits, Phys. Rev. B **77**, 174509 (2008).

[20] M. A. Ali Ahmed, G. A. Álvarez, and D. Suter, Robustness of dynamical decoupling sequences, Phys. Rev. A **87**, 042309 (2013).

[21] C. Zu, F. Machado, B. Ye, S. Choi, B. Kobrin, T. Mittiga, S. Hsieh, P. Bhattacharyya, M. Markham, D. Twitchen, A. Jarmola, D. Budker, C. R. Laumann, J. E. Moore, and N. Y. Yao, Emergent hydrodynamics in a strongly interacting dipolar spin ensemble, Nature (London) **597**, 45 (2021).

[22] B.-B. Wei, C. Burk, J. Wrachtrup, and R.-B. Liu, Magnetic ordering of nitrogen-vacancy centers in diamond via

resonator-mediated coupling, EPJ Quantum Technol. **2**, 18 (2015).
[23] T. R. Eichhorn, C. A. McLellan, and A. C. Bleszynski Jayich, Optimizing the formation of depth-confined nitrogen vacancy center spin ensembles in diamond for quantum sensing, Phys. Rev. Mater. **3**, 113802 (2019).
[24] H. Zhou, J. Choi, S. Choi, R. Landig, A. M. Douglas, J. Isoya, F. Jelezko, S. Onoda, H. Sumiya, P. Cappellaro, H. S. Knowles, H. Park, and M. D. Lukin, Quantum metrology with strongly interacting spin systems, Phys. Rev. X **10**, 031003 (2020).
[25] M. Joos, D. Bluvstein, Y. Lyu, D. Weld, and A. Bleszynski Jayich, Protecting qubit coherence by spectrally engineered driving of the spin environment, npj Quantum Inf. **8**, 47 (2022).
[26] D. Bluvstein, Z. Zhang, C. A. McLellan, N. R. Williams, and A. C. Bleszynski Jayich, Extending the quantum coherence of a near-surface qubit by coherently driving the paramagnetic surface environment, Phys. Rev. Lett. **123**, 146804 (2019).
[27] J. Zhang, P. W. Hess, A. Kyprianidis, P. Becker, A. Lee, J. Smith, G. Pagano, I.-D. Potirniche, A. C. Potter, A. Vishwanath, N. Y. Yao, and C. Monroe, Observation of a discrete time crystal, Nature (London) **543**, 217 (2017).
[28] E. L. Hahn, Spin echoes, Phys. Rev. **80**, 580 (1950).
[29] H. Y. Carr and E. M. Purcell, Effects of diffusion on free precession in nuclear magnetic resonance experiments, Phys. Rev. **94**, 630 (1954).
[30] S. Meiboom and D. Gill, Modified spin–echo method for measuring nuclear relaxation times, Rev. Sci. Instrum. **29**, 688 (1958).
[31] J. S. Waugh, L. M. Huber, and U. Haeberlen, Approach to high-resolution nmr in solids, Phys. Rev. Lett. **20**, 180 (1968).
[32] J. Choi, H. Zhou, H. S. Knowles, R. Landig, S. Choi, and M. D. Lukin, Robust dynamic Hamiltonian engineering of many-body spin systems, Phys. Rev. X **10**, 031002 (2020).
[33] C. P. Slichter, *Principles of Magnetic Resonance*, 3rd ed. (Springer-Verlag, Heidelberg, 1989).
[34] D. Li, Ph.D. thesis, Yale University, 2007.
[35] Y. Dong, R. G. Ramos, D. Li, and S. E. Barrett, Controlling coherence using the internal structure of hard π pulses, Phys. Rev. Lett. **100**, 247601 (2008).
[36] E. S. Petersen, A. M. Tyryshkin, K. M. Itoh, J. W. Ager, H. Riemann, N. V. Abrosimov, P. Becker, H. J. Pohl, M. L. W. Thewalt, and S. A. Lyon, Dynamical decoupling of interacting dipolar spin ensembles, arXiv:1807.04908.
[37] W. Zhang, N. Konstantinidis, K. A. Al-Hassanieh, and V. V. Dobrovitski, Modelling decoherence in quantum spin systems, J. Phys.: Condens. Matter **19**, 083202 (2007).
[38] E. D. Ostroff and J. S. Waugh, Multiple spin echoes and spin locking in solids, Phys. Rev. Lett. **16**, 1097 (1966).
[39] A. Ajoy, R. Nirodi, A. Sarkar, P. Reshetikhin, E. Druga, A. Akkiraju, M. McAllister, G. Maineri, S. Le, A. Lin, A. M. Souza, C. A. Meriles, B. Gilbert, D. Suter, J. A. Reimer, and A. Pines, Dynamical decoupling in interacting systems: Applications to signal-enhanced hyperpolarized readout, arXiv:2008.08323.
[40] C. D. Ridge, L. F. O'Donnell, and J. D. Walls, Long-lived selective spin echoes in dipolar solids under periodic and aperiodic π-pulse trains, Phys. Rev. B **89**, 024404 (2014).
[41] W. Hahn and V. V. Dobrovitski, Long-lived coherence in driven many-spin systems: From two to infinite spatial dimensions, New J. Phys. **23**, 073029 (2021).
[42] E. B. Fel'dman and S. Lacelle, Configurational averaging of dipolar interactions in magnetically diluted spin networks, J. Chem. Phys. **104**, 2000 (1996).
[43] J. R. Klauder and P. W. Anderson, Spectral diffusion decay in spin resonance experiments, Phys. Rev. **125**, 912 (1962).
[44] V. V. Dobrovitski, A. E. Feiguin, D. D. Awschalom, and R. Hanson, Decoherence dynamics of a single spin versus spin ensemble, Phys. Rev. B **77**, 245212 (2008).